

Interfacial Nanoinjection-Based Nanoliter Single-Cell Analysis

Juanli Yun, Xiaowei Zheng, Peng Xu, Xu Zheng, Jingyue Xu, Chen Cao, Yusi Fu, Bingxue Xu, Xin Dai, Yi Wang, Hongtao Liu, Qiaolian Yi, Yaxin Zhu, Jian Wang, Li Wang, Zhiyang Dong, Li Huang,* Yanyi Huang,* and Wenbin Du*

Single-cell analysis offers unprecedented resolution for the investigation of cellular heterogeneity and the capture of rare cells from large populations. Here, described is a simple method named interfacial nanoinjection (INJ), which can miniaturize various single-cell assays to be performed in nanoliter water-in-oil droplets on standard microwell plates. The INJ droplet handler can adjust droplet volumes for multistep reactions on demand with high precision and excellent monodispersity, and consequently enables a wide range of single-cell assays. Importantly, INJ can be coupled with fluorescence-activated cell sorting (FACS), which is currently the most effective and accurate single-cell sorting and isolation method. FACS-INJ pipelines for high-throughput plate well-based single-cell analyses, including single-cell proliferation, drug-resistance testing, polymerase chain reaction (PCR), reverse-transcription PCR, and whole-genome sequencing are introduced. This FACS-INJ pipeline is compatible with a wide range of samples and can be extended to various single-cell analysis applications in microbiology, cell biology, and biomedical diagnostics.

promoted the study of biological systems with respect to their physiological phenotypes,^[1] genomics,^[2,3] transcriptomics,^[4] epigenomics,^[5] proteomics,^[6] multiomics,^[7] and biodiversity^[8] at the single-cell level. Single-cell analysis allows the fundamental understanding of cell-to-cell heterogeneity and provides unprecedented resolution in complex biological systems, especially those from rare cell types or uncultivated microbes.^[9,10] However, current approaches for single-cell analysis usually involve complicated processes and instruments, require the use of microfabrication devices, and are cost-prohibitive for common laboratories.

In general, a single-cell analysis process can be divided into three major steps: single-cell isolation, reaction, and measurement. Single-cell isolation is the prerequisite step for single-cell analysis. Several systems have been commercialized with the capability of performing single-cell analysis with submicroliter to nanoliter volumes.^[11,12]


However, these systems are limited to certain cell types or confined to only one specific application or workflow. Microfluidic devices enable ultrahigh throughput isolation, reaction, and analysis of single cells.^[8,13,14] However, most microfluidic devices lack standardization which affects its world-to-chip interconnections and flexibility in coping with changes in applications. Currently,

1. Introduction

This paper describes interfacial nanoinjection (INJ), a simple microfluidic droplet-handling system developed for multi-step nanoliter assays on standard 96- or 384-well plates, and a simple pipeline that couples INJ and fluorescence-activated cell sorting (FACS) for single-cell analyses with high versatility, high throughput, and low cost. Recent research advances have

Dr. J. L. Yun, Dr. X. W. Zheng, Dr. P. Xu,^[†] J. Y. Xu, B. X. Xu, Dr. X. Dai, Y. Wang, H. T. Liu, Q. L. Yi, Y. X. Zhu, Dr. J. Wang, Dr. L. Wang, Prof. Z. Y. Dong, Prof. L. Huang, Prof. W. B. Du
 State Key Laboratory of Microbial Resources
 Institute of Microbiology
 Chinese Academy of Sciences
 Beijing 100101, China
 E-mail: huangl@im.ac.cn; wenbin@im.ac.cn
 Prof. X. Zheng
 State Key Laboratory of Nonlinear Mechanics
 Institute of Mechanics
 Chinese Academy of Sciences
 Beijing 100190, China

J. Y. Xu, B. X. Xu, H. T. Liu, Q. L. Yi, Prof. Z. Y. Dong, Prof. L. Huang, Prof. W. B. Du
 College of Life Sciences
 University of the Chinese Academy of Sciences
 Beijing 100049, China
 Dr. C. Cao,^[††] Dr. Y. S. Fu, Prof. Y. Y. Huang
 Biomedical Pioneering Innovation Center (BIOPIC)
 Beijing Advanced Innovation Center for Genomics (ICG)
 College of Engineering
 School of Life Sciences
 Peking-Tsinghua Center for Life Sciences
 Peking University
 Beijing 100871, China
 E-mail: huang@pku.edu.cn
 Prof. W. B. Du
 Savaid Medical School
 University of the Chinese Academy of Sciences
 Beijing 100049, China

 The ORCID identification number(s) for the author(s) of this article can be found under <https://doi.org/10.1002/sml.201903739>.

^[†]Present address: Bioengineering and Therapeutic Sciences, University of California, San Francisco, San Francisco, CA 94158, USA

^[††]Present address: Lewis-Sigler Institute for Integrative Genomics, Princeton University, Princeton, NJ 08540, USA

DOI: 10.1002/sml.201903739

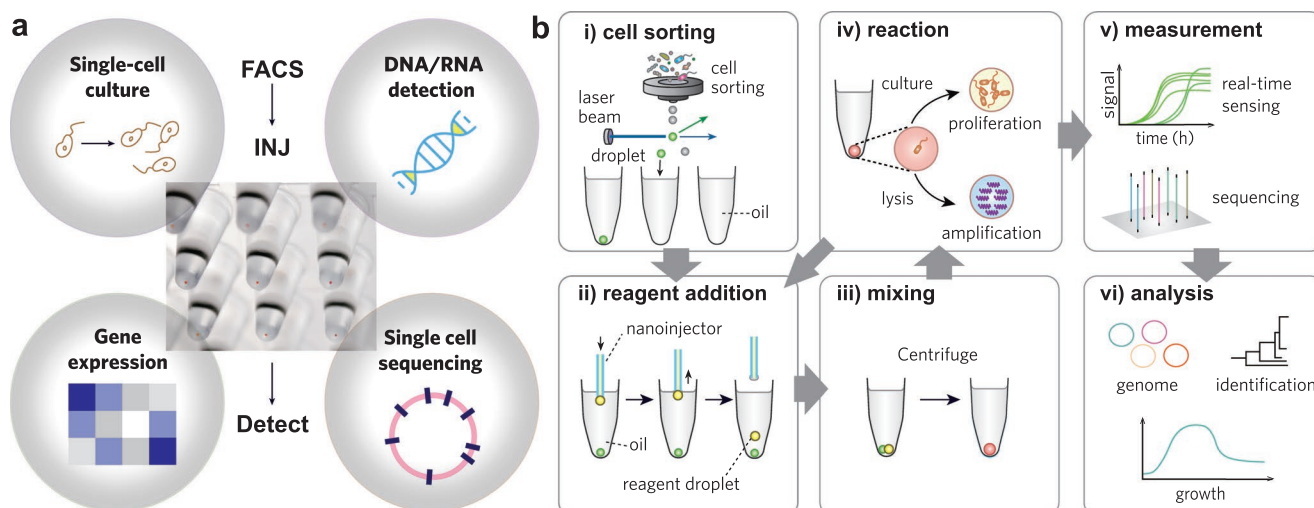


Figure 1. a) FACS-INJ pipeline and its single-cell analysis applications. b) General single-cell assay processed by FACS-INJ. i) single cells are sorted by FACS (MoFlo XDP, Beckman Coulter) into microwells preloaded with mineral oil. ii) Nanoliter volumes of reagents are added to the microwells by the INJ. iii) Droplets are coalesced in microwells by centrifugation (MINIP-2500, Miulab, Shanghai, China). iv) Droplets are incubated in different conditions for various single-cell assays, such as live-cell proliferation and molecular analysis. v) Single-cell assay results are measured by fluorescence readers (EnSpire, Perkin Elmer; or Vii7 Real-Time PCR thermocycler, Applied Biosystems), and amplified nucleic acids are subjected to next-generation sequencing. vi) Data analysis and interpretation.

flow cytometry, especially FACS, remains as the most widely used single cell isolation method. FACS enables high-throughput single-cell sorting with multiple dimensions and reduces contamination caused by the codeposition of extracellular contaminants.^[15,16] Moreover, FACS can sort single cells into standard microwell plates for single-cell cultivation, detection, or amplification, and the results can be read out using microscopes or plate readers. However, FACS is not compatible with state-of-art microfluidic platforms, and most of these FACS-based single-cell assays are performed at the microliter level, which is costly when a large number of single cells have to be studied. Scaling down a single-cell reaction to the nanoliter level is helpful to reduce the cost, minimize contamination,^[17,18] avoid dilution of minute amounts of cellular components (e.g., DNA, RNA, protein, and secretions), and reduce the assay time. Hitherto, a major unmet need is the lack of a miniaturized liquid handling system that can interface the upstream FACS and downstream measurements for high-throughput nanoliter single-cell assays. In this paper, we introduce INJ, which handles nanoliter droplets with high precision and allows multistep nanoliter assays on standard microwell plates. We coupled INJ with FACS and different commercial fluorescence readers and demonstrated the performance of the platform in various single-cell phenotypic and genotypic analyses, as well as whole-genome amplification (WGA). We believe that the FACS-INJ platform can provide simple, reliable, flexible, and versatile features for various single-cell analyses of both prokaryotic and eukaryotic cells.

2. Results

2.1. The FACS-INJ Pipeline

The overview workflow of the FACS-INJ system is shown in Figure 1a. It allows live-cell proliferation or cell-lysate analysis

such as DNA and RNA level gene amplification and detection (Figure 1a). Figure 1b illustrates the detailed procedures of single cell analyses with the FACS-INJ pipeline. First, single cells are sorted into oil-filled wells by FACS; afterward, nanoliter droplets containing different reagents are sequentially added to the wells by the INJ droplet handler (Figure S1, Supporting Information). A brief centrifugation step moves all the droplets to the well bottom, exerts kinetic energy to bring the droplets together, and forces the coalescence of droplets. The measurements of single-cell assays on microwell plates are performed by commercial fluorescence readers and followed by data analysis.

2.2. Nanoliter Droplet Handling with INJ

A simple automated droplet handler that applies the INJ technique was established using commercially available components (Figure S1, Supporting Information). The system consists of a syringe pump with a syringe, Teflon tubing attached to the syringe pump, a short fused-silica capillary sealed to the outlet of the tubing and vertically mounted to the Z translation stage, and an oil-filled microwell plate mounted on an XY translation stage. To use the droplet handler, the syringe pump is pre-filled with mineral oil, and microliters of reagents are aspirated into the Teflon tubing. The XY and Z stages are operated to insert the capillary tip into the oil-filled microwell, and nanoliter droplets down to 1 nL in volume can be injected into the oil by positive displacement of the pump. Then, the tip is pulled out of the surface of the oil in the well, and the droplet is pinched off the tip by the interfacial confinement and settles to the bottom of the well (Figure 2a,b and Movie S1, Supporting Information). The whole process is automated by a LabVIEW computer program, and the volume of droplets down to 1 nL can be customized for each well of the plate (Figure 2c and Movie S1,

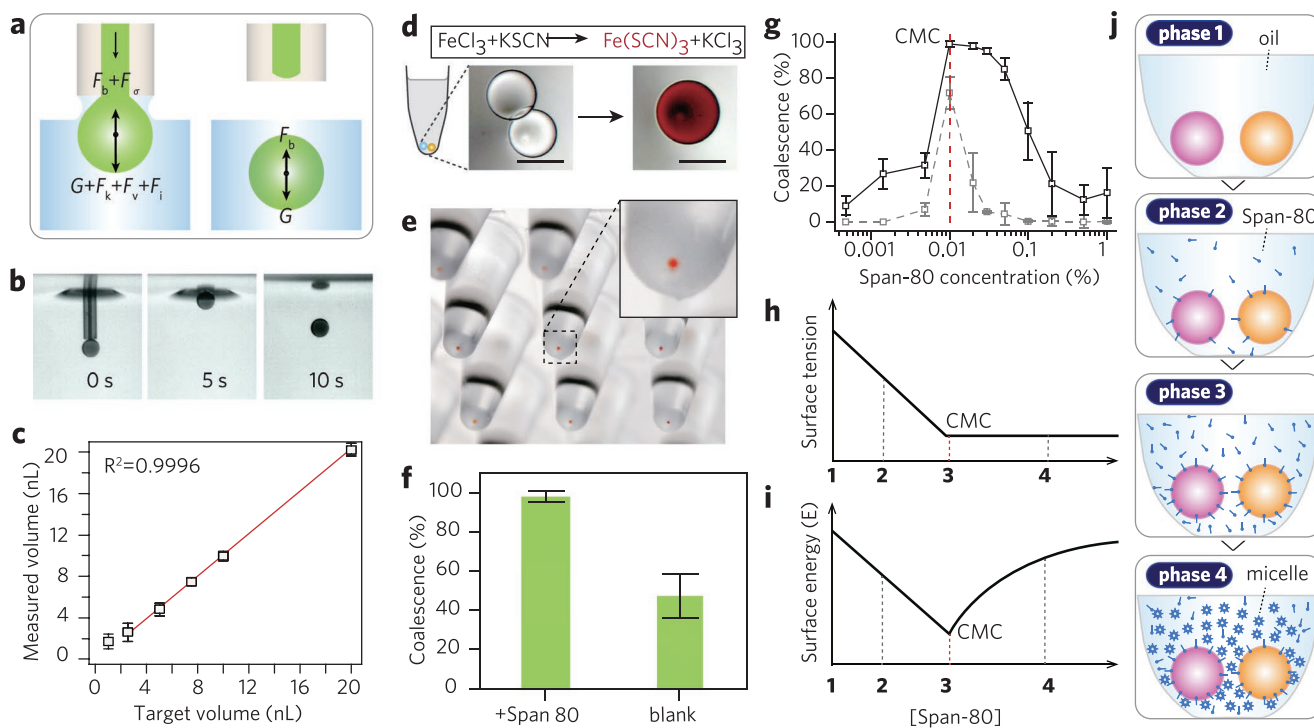


Figure 2. INJ performance in nanoliter droplet handling. a) Schematic illustration of the mechanism of droplet pinch-off from the tip of the capillary by INJ. b) Photomicrographs illustrating the generation of a 1 nL droplet by INJ at the mineral oil interface. c) Linear regression of injected and measured droplet volumes in the range of 1–20 nL. The error bars are the standard deviation of 25 replicates. d) Photomicrographs illustrating the coalescence of FeCl_3 and KSCN droplets in microwells after centrifugation, initiating the chromogenic reaction to produce an $\text{Fe}(\text{SCN})_2^+$ complex (red). Bars represent 200 μm . e) The coalescence of FACS-sorted droplets (≈ 2 nL, 0.1 M KSCN) with preloaded droplets (20 nL, 0.5 M FeCl_3) on a 96-well plate visualized by the chromogenic reaction. f) The coalescence ratio of FACS-sorted and preloaded droplets with or without the addition of Span-80 (0.01%). Error bars indicate the standard deviation for three 96-well plates ($n = 288$). g) Relationship between coalescence ratio and Span-80 concentration in mineral oil before (gray dashed line) and after centrifugation (solid black line). A consistent maximum coalescence rate was reached at 0.01–0.02% v/v Span-80 (red dashed line). The error bars are the standard deviations of three 96-well plates ($n = 288$). h–j) Schematic illustrations of the CMC-dependent coalescence of nanoliter droplets in microwells.

Supporting Information). The use of mineral oil prevents nanoliter droplet evaporation and contamination and provides a biocompatible environment for various single-cell analyses. 96- or 384-well plates with V-shaped bottoms allows convergence of multiple droplets at the bottom of the well upon centrifugation, yielding a coalescence ratio of 99.2% ($n = 288$) for 5 nL droplets (Figure 2d,g), and a 97.9% ($n = 288$) coalescence ratio of the FACS-sorted droplets (≈ 2 nL) with a preloaded 20 nL droplets (Figure 2e,f). More details for optimization and performance of droplet handling are provided in the Supporting Information.

2.3. Single-Cell Phenotypic Analysis

To demonstrate that the FACS-INJ pipeline is compatible with the single-cell phenotypic analysis, we selected *Escherichia coli* (*E. coli*) ATCC 25922 as a model strain for single-cell culture and measurement of the minimum inhibitory concentration (MIC) at the single-cell level. We used resazurin as a sensitive fluorescence indicator for bacterial proliferation.^[19] We optimized the droplet volume for cell cultivation in Luria broth containing 0.01% w/v resazurin (Figure S3, Supporting Information) and found that a 100 nL droplet volume yielded stable fluorescence profiles for dynamic *E. coli*

single-cell growth monitoring (Figure 3b and Figure S3, Supporting Information). Next, we sorted single *E. coli* cells into 384-well plates and performed antimicrobial susceptibility

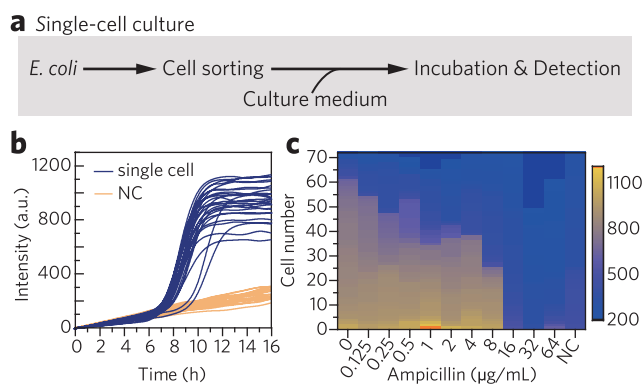


Figure 3. Single-cell cultivation and AST. a) FACS-INJ single-cell culture workflow. b) The growth curves of single *E. coli* cells. Both single-cell and negative control results include 103 replicates. c) The heatmap shows the endpoint fluorescence intensity (16 h) of 72 replicate wells at different antibiotic (ampicillin) concentrations. NC, no-cell control wells. The increased fluorescence intensity indicates increased cell growth at the corresponding ampicillin concentration. There is no growth when the fluorescence intensity is less than 500.

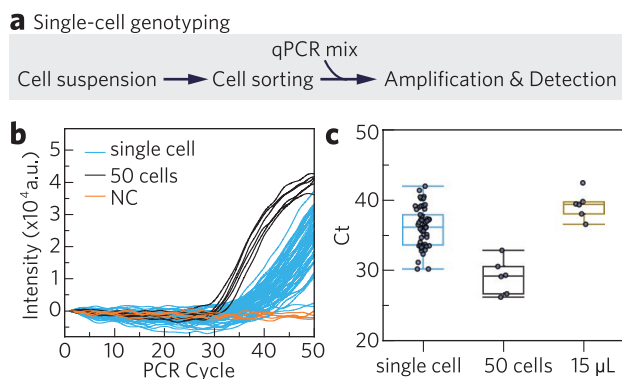


Figure 4. a) FACS-INJ workflow for single-cell genotyping based on Taqman PCR. b) Taqman qPCR amplification curves and c) C_t value comparison for single cells in 800 nL ($n = 60$), 50 cells in 800 nL ($n = 6$), and single cells in 15 μL ($n = 6$) volumes.

testing (AST) on the single cells to measure the MIC of ampicillin against *E. coli*. As shown in Figure 3c, the percentage of growth of single cells decreased with increasing concentrations of ampicillin, and no cells grew in the presence of 16 $\mu\text{g mL}^{-1}$ ampicillin, which was determined as the MIC. The single-cell AST result is consistent with the conventional AST result on microwell plates. In comparison, our method consumes 2000 times fewer reagents than conventional plate assays (200 μL) and, more importantly, provides population-level statistical analysis to characterize physiological responses of individual cells to culture conditions, antibiotics, and chemicals.

2.4. Single-Cell Genotypic Analysis

To enable single-cell genotyping and pathogen detection, we used the FACS-INJ system to perform polymerase chain reaction (PCR)-based nucleic acid amplification of antibiotic-resistance genes of the pathogenic bacteria *Acinetobacter baumannii* (Figure 4a). In total, 104 single cells were sorted and amplified by using quantitative real-time PCR with $bla_{\text{OXA-51}}$ gene-specific primers and a TaqMan probe. The amplification resulted in 188 bp amplicons for the $bla_{\text{OXA-51}}$ targeted site, which encodes beta-lactamase in *A. baumannii*.

We scaled down the PCR volume to 800 nL, as shown in the real-time fluorescence curves in Figure 4b. The target sequences were amplified in 59 out of 104 reactions. In order to confirm the specificity of the $bla_{\text{OXA-51}}$ gene detection, we also set up negative controls using *Pseudomonas aeruginosa* PAO1 single cell lysate and no amplification was observed in 80 replicates, indicating the specificity of our antibiotic resistant gene measurement. Compared with the conventional PCR in a 15 μL volume ($n = 15$), the nanoliter reaction shows higher sensitivity (Figure 4c) with a lower C_t value ($\Delta C_t = 2.23$, based on the mean C_t value of each volume). The overall single-cell PCR amplification success rate was 56.7%, which is consistent with previous studies.^[20,21] We also ran a cell number-based amplification for comparison with the single-cell PCR. The 10-cell PCR showed an overall 91.7% (44 of 48) success rate, the 50-cell PCR amplification showed

an overall 96.9% (31 of 32) success rate, and no amplification was detected in the no-cell control reactions (Figure 4b). The ΔC_t between 10 cells and single cells was 5.56 ± 1.0 , and that between 50 cells and single cells was 6.93 ± 0.3 . As FACS allows selective sorting of rare pathogens in complex samples such as blood and cerebrospinal fluid, the single-cell PCR tests can provide culture-free rapid identification of pathogenic bacteria and fungi as well as their drug resistance genes of infectious diseases at early stage.

2.5. Single-Cell Gene Expression

To demonstrate the single-cell gene expression analysis capability of FACS-INJ, we measured the inflammatory response of mouse macrophage RAW264.7 cells treated with bacterial lipopolysaccharide (LPS) at the RNA level with multiplexed one-step reverse-transcription PCR (RT-PCR). Previous studies have shown that LPS, a major outer membrane component of gram-negative bacteria, is an endotoxin that induces the macrophage inflammatory response to release proinflammatory cytokines, including interleukin-1 β (IL-1 β),^[22] which is indicated by the upregulation of the expression of the IL-1 β coding gene. To measure IL-1 β gene expression with or without LPS treatment, we designed a duplexed RT-PCR system to detect the expression of the IL-1 β gene and the housekeeping gene hypoxanthine guanine phosphoribosyltransferase (HPRT) as an internal reference. Single RAW264.7 cells with or without LPS treatment were sorted and merged with the RT-PCR mix for the real-time RT-PCR analysis (Figure 5a). In the optimal reaction volume of 600 nL (Figure 5a and Figure S4, Supporting Information), HPRT showed consistent expression in both LPS-treated and untreated cells, while IL-1 β expression in single cells treated with LPS was significantly upregulated compared to that of untreated cells (Figure 5b–d). This FACS-INJ-based single-cell RT-PCR can be applied to analyze the gene expression of mammalian cells, plant cells, and microorganisms.

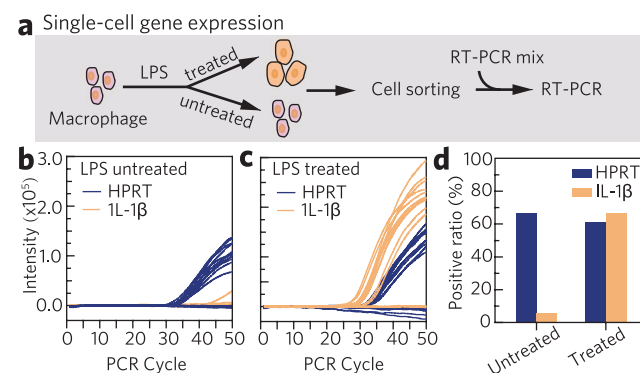


Figure 5. a) Single-cell gene expression workflow based on FACS. The mouse macrophage cell line RAW264.7 was treated with either LPS or medium, and the inflammatory response of a single cell was measured by one-step RT-PCR using the FACS-INJ system. b,c) RT-PCR detection of HPRT and IL-1 β gene expression levels in macrophages treated with b) medium or c) 100 ng mL^{-1} LPS for 16 h. d) Single-cell IL-1 β gene expression profiling with and without LPS treatment.

2.6. Single-Cell Sequencing

To enable the single-cell sequencing of uncultivable microorganisms, we developed a single-cell multiple displacement amplification (MDA) pipeline based on FACS-INJ, evaluated its performance with a benchmark strain, and applied it to the WGA of deep-sea microorganisms. MDA has been widely used for single-cell WGA due to its high recovery rate and accuracy.^[23] As shown in **Figure 6a**, the workflow involves sorting, lysis, neutralization, amplification, and phylogenetic identification steps. These steps of the optimal procedure require the addition of nanoliter droplets of the corresponding reagent ranging from 20 to 300 nL in volume, with a final reaction volume of 360 nL. SYBR Green was added to the amplification mix to allow real-time monitoring of single-cell MDA and the selection of positive reactions for subsequent sequencing and phylogenetic identification (Figures 1 and 6a).

To optimize the single-cell MDA and control for contamination, we evaluated the performance of a series of volumes ranging from 160 to 1060 nL using *Sulfolobus* sp. A20 (an archaeal

strain isolated from an acidic hot spring in Laguna Fumárica, Costa Rica^[24]) as the benchmark strain (Figure 6b–d). For each volume, we used 100 cells as positive controls and no cells as negative controls. Based on the critical point (Cp) of the real-time amplification curves of the single cells and controls, we obtained an optimal reaction volume of 360–560 nL, for which Cps from single cells and positive controls (<3 h) can be distinguished from those of the negative controls (>3 h), indicating successful amplification of a single cell without contamination. We found that reaction volumes greater than 660 nL introduce serious contamination (Figure 6b and Figures S5 and S6, Supporting Information). These results confirm that single-cell MDA in reduced nanoliter volumes can effectively decrease the risks of the off-target amplification of contaminants.^[3,17]

To further assess the performance of single-cell MDA, we sent the products of successful reactions in different volumes for sequencing and obtained ≈600 million reads from each amplification product to produce single-cell genome assemblies. The results revealed that the average whole-genome

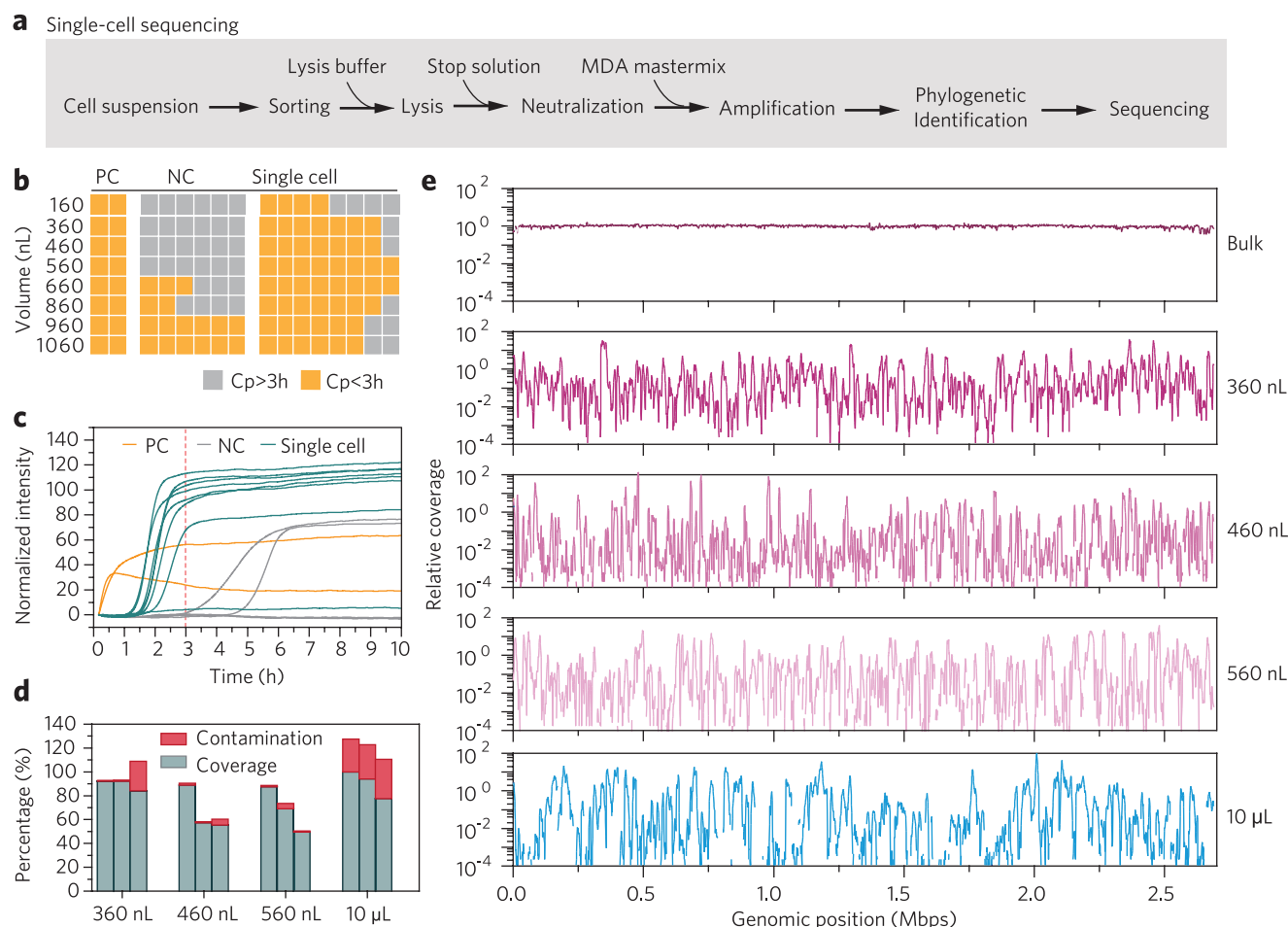


Figure 6. Single-cell whole-genome MDA amplification with the benchmark strain *Sulfolobus* sp. A20. a) Workflow. b) Optimization of the MDA reaction volume from 110 to 1060 nL. Each square represents one replicate for each reaction volume. PC indicates replicates with 100 cells, and NC is the negative control without cells. c) Real-time fluorescence curves for single *Sulfolobus* sp. A20 cell MDA in a 360 nL reaction volume. d) Genome coverage and contamination of each assembly. Error bars are the standard deviation of three replicates. e) The evenness of representative single-cell assemblies in different reaction volumes.

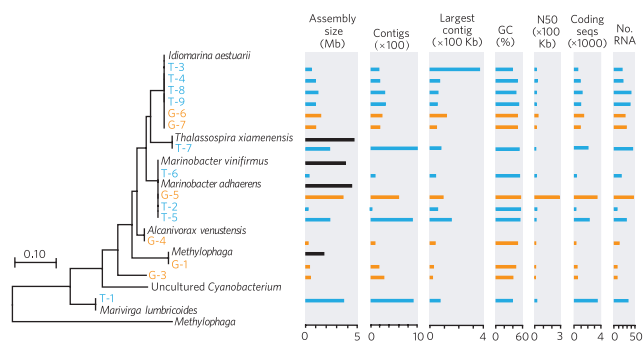


Figure 7. Phylogenetic assignment and annotation details of Southwest Indian Sea sediment single-cell assemblies. Blue and orange bars represent single cells from sedimentary Tombarthite (T) and a sediment core collected using a gravity column sampler (G), respectively. Black bars represent reference genomes in the National Center for Biotechnology Information database.

coverage for 360, 460, and 560 nL single-cell MDA was 79.0%, 55.4%, and 61.3%, respectively. The genome coverage was not significantly different from that obtained in 10 μ L reaction volumes (65.2%). However, the contamination ratio for the nanoliter MDA in the range of 360–560 nL was less than 5% (Figure 6d), which is significantly better than that of the 10 μ L volume reactions (Figure 6d and Table S2, Supporting Information). Moreover, MDA in nanoliter volumes presented better evenness of WGA than that in the 10 μ L volume (Figure 6e and Figure S7, Supporting Information), which is consistent with the results of previous microfluidic-based single-cell MDA studies.^[2,3,17,25]

To assess the performance of single-cell MDA in retrieving the whole genome sequences of uncultivated microbes, two deep-sea sediment samples from the Southwest Indian Ocean, including a sedimentary Tombarthite (T) and a sediment core collected with a gravity column sampler (G), were used for single-cell MDA at optimal 360–560 nL volumes. After phylogenetic identification, 15 single-cell MDA products (9 from T and 6 from G samples) were sequenced and each yielded \approx 2 Gb paired-end reads. As shown in Figure 7, the sizes of the assemblies ranged from 0.21 to 3.67 Mbp, and the genome completeness was estimated to vary from 6.04% to 73.5% (Figure S8a, Supporting Information). Compared to previous single-cell MDA methods,^[3,10,25] the FACS-INJ pipeline produces comparable assembly size and completeness with markedly lower contamination levels (<5%), indicating that our single-cell WGA is robust and compatible with environmental samples. We also found large numbers of carbohydrate-active enzymes (CAZymes) in all single-cell genome assemblies (Figure S8b, Supporting Information), indicating that these microbes potentially function in carbon cycling in deep oceans.

3. Discussion

Here, we describe FACS-INJ, a new platform that combines INJ droplet handling with FACS for high-throughput single-cell analyses in nanoliter volumes. FACS provides multidimensional selectivity of target cells as well as compatibility with various types of single-cell assays (Figure 1a). INJ provides

many advantages over other microfluidic methods. First, only a syringe pump and a compact automated translation stage are required for the assembly of the INJ droplet handler, which can be easily established in common laboratories with commercially available components. Second, droplets of volumes down to 5 nL can be generated with high accuracy on demand (Figure 2c) in standard well plates. Third, multistep assays can be performed in nanoliter volumes by sequential INJ of nanoliter droplets of different reagents, followed by efficient coalescence by centrifugation and simple measurement gathering using fluorescence plate readers or real-time PCR machines (Figure 1b and Figure S1, Supporting Information).

The mechanism of droplet pinch-off from the tip of the capillary by INJ is similar to that of our previously reported interfacial emulsification method,^[26,27] which continuously generates monodisperse picoliter to nanoliter droplets at throughput speeds of 50 to 500 droplets per second and has been used for digital nucleic acid amplification,^[28] polymeric microparticle synthesis,^[29] and AST.^[30] Briefly, at the very moment the capillary moves out of the oil phase, several forces, including the water–oil interfacial tension F_σ , the viscous drag force F_v , the gravity G , the buoyancy F_b , the kinetic force F_k , and the interfacial confinement force F_i , affect the detachment of the droplet. Among these forces, the confinement force of the water–oil interface, originating from the interfacial tension resisting deformation of the interface during the elevation of the capillary, is the decisive force that overcomes all barrier forces (including F_σ and F_b) against detachment.^[26] We evaluate that the force F_i is much larger than the barrier forces $F_\sigma + F_b$, which makes the droplet detachment easy and reproducible. The droplet then settles to the bottom of the well.

The coalescence of nanoliter droplets in microwell plates, which is achieved by the combined effects of the surfactant Span-80 and centrifugation, is the key for the success of multistep single-cell assays. The droplet coalescence ratio at different Span-80 concentrations before and after centrifugation was evaluated by the chromogenic reaction of two 5 nL droplets (Figure 2g). Notably, centrifugation is necessary for fast coalescence (1 min), as it provides kinetic energy for the droplets in the bottom of a microwell to collide with each other, which allows for robust high-throughput analysis. The addition of Span-80 dramatically reduces the surface tension to enhance the coalescence ratio at the critical micelle concentration (CMC), which is 0.01–0.02% v/v (Figure 2d–j). This finding indicates a CMC-dependent coalescence. Generally, the coalescence ratio of droplets is determined by the change in surface energy (Figure 2h,i).

As the Span-80 concentration increases from 0 to the CMC (phase 1–3, Figure 2j), the surface tension gradually decreases, as does the surface energy (E) of the system, which is defined as $n\sigma A$ (where n is the number of droplets in a microwell, $A = 4\pi r^2$ is the surface area of a single droplet). As a result, the coalescence ratio reaches its highest value, which is up to 99.2% with centrifugation, as shown in Figure 2g. When the concentration of Span-80 exceeds the CMC, the surfactant molecules form micelles in the oil solution rather than staying at the interfacial layer of the droplet. In contrast, these micelles in the oil solution prevent the coalescence of the droplets, as they exist between the droplet surfaces and increase the surface energy

($E = nA + A_m$, where A_m is the total surface of the micelles in the oil solution). The blockage effect of these micelles is not fully eliminated by centrifugation, as shown by the lower coalescence ratio than that observed at CMC (phase 4, Figure 2j).

Despite the convenient manipulation and accuracy, FACS-INJ is compatible with most single-cell assays at minimized volume. For example, we used the platform for single-cell phenotypic analysis, genotypic analysis, gene expression analysis, and whole-genome sequencing. All these applications display comparable sensitivity or coverage to that of conventional procedures at microliter volumes, but with greatly reduced reagent consumption and ratios of contamination. The minimized analysis not only is cost-effective but also enables biological research and medical diagnosis based on single-cell analyses. The single-cell AST may provide accurate dose guidance for clinical diagnosis, especially when the available specimen is limited, and reveal the heterogeneous drug resistance landscape of pathogens. The detection of DNA and RNA in single cells with PCR and RT-PCR reveals many opportunities in single-cell genotyping, functional identification, and genetic diagnosis of diseases such as sepsis and cancer. Single-cell MDA provides a streamlined workflow for high-throughput single-cell genome sequencing of uncultured microorganisms, as well as circulating tumor cells, thereby may promote the prevalence of individualized precision medicine.

4. Conclusion

In summary, we have developed INJ, a nanoliter droplet handler that allows high-throughput nanoliter assays on micro-well plates without a complicated setup or microfabricated devices. Compared with conventional positive-displacement pipetting systems, INJ reduces handling volumes down to the nanoliter level with high precision and reproducibility and is compatible with standard 96- or 384-well plates for automated and high-throughput assays and screening. Importantly, INJ is compatible with commercial FACS and allows us to establish programmable and configurable FACS-INJ pipelines for various single-cell analyses at the nanoliter level. FACS-INJ allows accurate and efficient sorting, isolation, reaction, and measurement of single cells at high-throughput with nanoliter reagent consumption and is versatile, precise, cost-effective, and robust. We recruit FACS as single-cell sorter because FACS allows sorting of particles from 100 nm to several hundred microns, which allows single cell sorting and analysis of viruses,^[31] bacteria,^[32] yeasts,^[33–35] and mammalian cells or multi-cellular organoids. With its high resolution, FACS is capable of distinguishing cells from heterogeneous populations based on cell size, shape, cellular content, and phenotypes,^[34–36] which shows much higher flexibility than other methods.^[37]

Compared with current microfluidic-based single-cell analysis methods which can analyze thousands to tens of thousands of cells in one run, the throughput of FACS-INJ is limited to several hundreds per plate. However, split-pool barcoding method^[38] might be integrated to increase the throughput of single cell analysis using FACS-INJ exponentially. Furthermore, the FACS-INJ brings four advantages: i) Compatibility with standardized well plates and detecting facilities; ii) no limitation

in number of assay steps and high flexibility to change in demand; iii) high efficiency and specificity in single-cell sorting and selection provided by FACS; iv) no restriction on cell sizes and overcoming limitation of Poisson distribution and multi-cell events. Compared with other plate-based miniaturization techniques, the FACS-INJ method avoids the disturbance of external forces such as acoustic ejection^[11,12] and contamination due to surface contact or evaporation,^[39] and allows single-cell assays to be scaled down to tens to hundreds nanoliters on standard well plates.

The detection systems used in this work are common real-time PCR machines or fluorescence plate readers that are widely available. To further reduce the reaction volume of single-cell assays from hundreds of nanoliters to tens of nanoliters, we may use high-resolution and high-sensitivity fluorescence microscopes or customized fluorescence detection systems. We may also extend the detection methods to include electrochemical detectors or chemiluminescence for other applications, such as single-cell immunoassays. In addition to single-cell analysis, FACS-INJ also allows the sorting of different cell types in the same microwell with high selectivity, thus creating great opportunities for cell–cell interaction studies. We believe that the FACS-INJ method is widely applicable for single-cell analysis in microbiology, cell biology, and clinical diagnosis.

5. Experimental Section

See the Supporting Information for the detailed experimental procedures and materials.

Supporting Information

Supporting Information is available from the Wiley Online Library or from the author.

Acknowledgements

J.Y., X.Z., and P.X. contributed equally to this work. W.D., L.H., and Y.H. conceived the project; W.D., L.H., Y.H., J.Y., P.X., X.W.Z., J.X., X.D., J.W., L.W., and Z.D. designed all experiments; W.D., J.Y., P.X., X.W.Z., Y.W., and Q.Y. built and optimized the INJ platform; X.Z. and W.D. built the physical model of INJ; X.W.Z., Y.Z., J.W., and Z.D. collected deep-sea sediment samples; J.Y., P.X., X.W.Z., B.X., Y.W., C.C., and Y.F. performed single-cell MDA experiments and bioinformatic analysis; J.X. performed live-cell analysis experiments and gene expression experiments; W.D., J.Y., P.X., X.W.Z., X.Z., and L.H. wrote the manuscript. This work was financially supported by China Ocean Mineral Resources R&D Association (DY135-B2-02), National Natural Science Foundation of China (41977196, 21822408, 21525521, 11832017, 11572335), National Key R&D Program of China (2016YFE0205800, 2016YFC0100900, 2018YFC0310703), the Chinese Academy of Sciences (XDB15040102, QYZDB-SSW-SMC008, QYZDB-SSW-JSC036, KFZD-SW-219-4, XDB22040403), and the State Key Laboratory of Microbial Resources, Institute of Microbiology, Chinese Academy of Sciences (SKLMR-20150602).

Conflict of Interest

The authors declare no conflict of interest.

Keywords

droplet, fluorescence-activated cell sorting, microfluidics, single-cell analysis, single-cell sequencing

Received: July 14, 2019
Revised: September 8, 2019
Published online:

- [1] J. H. Levine, E. F. Simonds, S. C. Bendall, K. L. Davis, E. Amir, M. D. Tadmor, O. Litvin, H. G. Fienberg, A. Jager, E. R. Zunder, R. Finck, A. L. Gedman, I. Radtke, J. R. Downing, D. Pe'Er, G. P. Nolan, *Cell* **2015**, *162*, 184.
- [2] Y. Marcy, C. Ouverney, E. M. Bik, T. Losekann, N. Ivanova, H. G. Martin, E. Szeto, D. Platt, P. Hugenholtz, D. A. Relman, S. R. Quake, *Proc. Natl. Acad. Sci. USA* **2007**, *104*, 11889.
- [3] F. Lan, B. Demaree, N. Ahmed, A. R. Abate, *Nat. Biotechnol.* **2017**, *35*, 640.
- [4] D. A. Jaitin, E. Kenigsberg, H. Keren-Shaul, N. Elefant, F. Paul, I. Zaretsky, A. Mildner, N. Cohen, S. Jung, A. Tanay, I. Amit, *Science* **2014**, *343*, 776.
- [5] G. Kelsey, O. Stegle, W. Reik, *Science* **2017**, *358*, 69.
- [6] J. R. Newman, S. Ghaemmaghami, J. Ihmels, D. K. Breslow, M. Noble, J. L. DeRisi, J. S. Weissman, *Nature* **2006**, *441*, 840.
- [7] S. Bian, Y. Hou, X. Zhou, X. Li, J. Yong, Y. Wang, W. Wang, J. Yan, B. Hu, H. Guo, J. Wang, S. Gao, Y. Mao, J. Dong, P. Zhu, D. Xiu, L. Yan, L. Wen, J. Qiao, F. Tang, W. Fu, *Science* **2018**, *362*, 1060.
- [8] S. S. Terekhov, I. V. Smirnov, A. V. Stepanova, T. V. Bobik, Y. A. Mokrushina, N. A. Ponomarenko Jr., A. A. Belogurov, M. P. Rubtsova, O. V. Kartseva, M. O. Gomzikova, A. A. Moskovtsev, A. S. Bukatin, M. V. Dubina, E. S. Kostryukova, V. V. Babenko, M. T. Vakhitova, A. I. Manolov, M. V. Malakhova, M. A. Kornienko, A. V. Tyakht, A. A. Vanyushkina, E. N. Ilina, P. Masson, A. G. Gabibov, S. Altman, *Proc. Natl. Acad. Sci. USA* **2017**, *114*, 2550.
- [9] C. C. Ooi, G. L. Mantalas, W. Koh, N. F. Neff, T. Fuchigami, D. J. Wong, R. J. Wilson, S. M. Park, S. S. Gambhir, S. R. Quake, S. X. Wang, *PLoS One* **2017**, *12*, e188510.
- [10] R. Stepanauskas, E. A. Fergusson, J. Brown, N. J. Poulton, B. Tupper, J. M. Labonte, E. D. Becraft, J. M. Brown, M. G. Pachiadaki, T. Povilaitis, B. P. Thompson, C. J. Mascena, W. K. Bellows, A. Lubys, *Nat. Commun.* **2017**, *8*, 84.
- [11] J. Olechno, R. Stearns, R. Ellson, E. Heron, *Innovations Pharm. Technol.* **2006**, *19*, 40.
- [12] S. Mora-Castilla, C. To, S. Vaezeslami, R. Morey, S. Srinivasan, J. N. Dumdie, H. Cook-Andersen, J. Jenkins, L. C. Laurent, *J. Lab. Autom.* **2016**, *21*, 557.
- [13] D. S. Tawfik, A. D. Griffiths, *Nat. Biotechnol.* **1998**, *16*, 652.
- [14] S. S. Terekhov, I. V. Smirnov, M. V. Malakhova, A. E. Samoilov, A. I. Manolov, A. S. Nazarov, D. V. Danilov, S. A. Dubiley, I. A. Osterman, M. P. Rubtsova, E. S. Kostryukova, R. H. Ziganshin, M. A. Kornienko, A. A. Vanyushkina, O. N. Bukato, E. N. Ilina, V. V. Vlasov, K. V. Severinov, A. G. Gabibov, S. Altman, *Proc. Natl. Acad. Sci. USA* **2018**, *115*, 9551.
- [15] C. Rinke, J. Lee, N. Nath, D. Goudeau, B. Thompson, N. Poulton, E. Dmitrieff, R. Malmstrom, R. Stepanauskas, T. Woyke, *Nat. Protoc.* **2014**, *9*, 1038.
- [16] A. Aharoni, K. Thieme, C. P. Chiu, S. Buchini, L. L. Lairson, H. Chen, N. C. Strynadka, W. W. Wakarchuk, S. G. Withers, *Nat. Methods* **2006**, *3*, 609.
- [17] Y. Marcy, T. Ishoey, R. S. Lasken, T. B. Stockwell, B. P. Walenz, A. L. Halpern, K. Y. Beeson, S. M. Goldberg, S. R. Quake, *PLoS Genet.* **2007**, *3*, e155.
- [18] C. R. Hutchison, H. O. Smith, C. Pfannkoch, J. C. Venter, *Proc. Natl. Acad. Sci. USA* **2005**, *102*, 17332.
- [19] R. Agren, L. Liu, S. Shoae, W. Vongsangnak, I. Nookaew, J. Nielsen, *PLoS Comput. Biol.* **2013**, *9*, e1002980.
- [20] K. Leung, H. Zahn, T. Leaver, K. M. Konwar, N. W. Hanson, A. P. Page, C. C. Lo, P. S. Chain, S. J. Hallam, C. L. Hansen, *Proc. Natl. Acad. Sci. USA* **2012**, *109*, 7665.
- [21] R. Tewhey, J. B. Warner, M. Nakano, B. Libby, M. Medkova, P. H. David, S. K. Kotsopoulos, M. L. Samuels, J. B. Hutchison, J. W. Larson, E. J. Topol, M. P. Weiner, O. Harismendy, J. Olson, D. R. Link, K. A. Frazer, *Nat. Biotechnol.* **2009**, *27*, 1025.
- [22] S. Guan, H. Feng, B. Song, W. Guo, Y. Xiong, G. Huang, W. Zhong, M. Huo, N. Chen, J. Lu, X. Deng, *Int. Immunopharmacol.* **2011**, *11*, 2194.
- [23] F. B. Dean, S. Hosono, L. Fang, X. Wu, A. F. Faruqi, P. Bray-Ward, Z. Sun, Q. Zong, DuY, DuJ, M. Driscoll, W. Song, S. F. Kingsmore, M. Egholm, R. S. Lasken, *Proc. Natl. Acad. Sci. USA* **2002**, *99*, 5261.
- [24] X. Dai, H. Wang, Z. Zhang, K. Li, X. Zhang, M. Mora-Lopez, C. Jiang, C. Liu, L. Wang, Y. Zhu, W. Hernandez-Ascencio, Z. Dong, L. Huang, *Front. Microbiol.* **2016**, *7*, 1902.
- [25] M. Hosokawa, Y. Nishikawa, M. Kogawa, H. Takeyama, *Sci. Rep.* **2017**, *7*, 5199.
- [26] P. Xu, X. Zheng, Y. Tao, W. Du, *Anal. Chem.* **2016**, *88*, 3171.
- [27] S. L. Liao, Y. Tao, W. B. Du, Y. P. Wang, *Langmuir* **2018**, *34*, 11655.
- [28] Y. Hu, P. Xu, J. Luo, H. He, W. Du, *Anal. Chem.* **2017**, *89*, 745.
- [29] S. Liao, Y. He, D. Wang, L. Dong, W. Du, Y. Wang, *Adv. Mater. Technol.* **2016**, *1*, 1600021.
- [30] S. L. Liao, X. L. Tao, Y. J. Ju, J. Feng, W. B. Du, Y. P. Wang, *ACS Appl. Mater. Interfaces* **2017**, *9*, 4345.
- [31] S. Sokolenko, J. Nicastro, R. Slavcev, M. G. Aucoin, *Cytometry, Part A* **2012**, *81A*, 1031.
- [32] L. Wu, Y. Song, T. Luan, L. Ma, L. Su, S. Wang, X. Yan, *Biosens. Bioelectron.* **2016**, *86*, 102.
- [33] E. T. Boder, K. D. Wittrup, *Nat. Biotechnol.* **1997**, *15*, 553.
- [34] H. Zhang, A. Torkamani, T. M. Jones, D. I. Ruiz, J. Pons, R. A. Lerner, *Proc. Natl. Acad. Sci. USA* **2011**, *108*, 13456.
- [35] A. Rajpal, N. Beyaz, L. Haber, G. Cappuccilli, H. Yee, R. R. Bhatt, T. Takeuchi, R. A. Lerner, R. Crea, *Proc. Natl. Acad. Sci. USA* **2005**, *102*, 8466.
- [36] R. A. Lerner, *Angew. Chem., Int. Ed.* **2006**, *45*, 8106.
- [37] A. Gross, J. Schoendube, S. Zimmermann, M. Steeb, R. Zengerle, P. Koltay, *Int. J. Mol. Sci.* **2015**, *16*, 16897.
- [38] A. B. Rosenberg, C. M. Roco, R. A. Muscat, A. Kuchina, P. Sample, Z. Yao, L. T. Graybuck, D. J. Peeler, S. Mukherjee, W. Chen, S. H. Pun, D. L. Sellers, B. Tasic, G. Seelig, *Science* **2018**, *360*, 176.
- [39] W. Gaisford, G. Schertler, P. Edwards, *Nat. Methods* **2011**, *8*, 520.